ANALYSIS OF A CANARD MECHANISM BY WHICH EXCITATORY SYNAPTIC COUPLING CAN SYNCHRONIZE NEURONS AT LOW FIRING FREQUENCIES*

JONATHAN DROVER†, JONATHAN RUBIN†, JIANZHONG SU‡, AND
BARD ERMENTROUT†

Abstract. A population of oscillatory Hodgkin–Huxley (HH) model neurons is shown numerically to exhibit a behavior in which the introduction of excitatory synaptic coupling synchronizes and dramatically slows firing. This effect contrasts with the standard theory that recurrent synaptic excitation promotes states of rapid, sustained activity, independent of intrinsic neuronal dynamics. The observed behavior is not due to simple depolarization block nor to standard elliptic bursting, although it is related to these phenomena. We analyze this effect using a reduced model for a single, self-coupled HH oscillator. The mechanism explained here involves an extreme form of delayed bifurcation in which the development of a vortex structure through interaction of fast and slow subsystems pins trajectories near a surface that consists of unstable equilibria of a certain reduced system, in a canard-like manner. Using this vortex structure, a new passage time calculation is used to approximate the interspike time interval. We also consider how changes in the synaptic opening rate can modulate oscillation frequency and can lead to a related scenario through which bursting may occur for the HH equations as the synaptic opening rate is reduced.

Key words. neuronal oscillations, Hodgkin–Huxley equations, synaptic excitation, slow passage, canard

AMS subject classifications. 34C15, 34C23, 34C25, 37G15, 37N25, 92C20

DOI. 10.1137/S0036139903431233

1. Introduction. Recurrent excitatory networks of neurons are purported to underlie persistent activity in the nervous system. Such networks have been used as models for wave propagation and short-term memory [2, 17]. Long-lasting excitatory synaptic connectivity is generally sufficient to enable such densely coupled neurons to fire repetitively at high rates after some transient input, even when the individual neurons do not intrinsically oscillate. The ability of an excitatory network to maintain a persistent state depends on several interacting factors. In many types of cortical neuron models, excitatory coupling leads to asynchronous firing when the synaptic time course lasts long enough [10]. Shortening the time constant leads to two effects; first, the neurons can synchronize, and second, thus synchronized, the network cannot reignite due to the refractory period of the neurons. Studies of persistent activity have not generally focused on differences from this standard scenario that arise due to the intrinsic dynamics of individual neurons.

In this paper we report on a new mechanism through which persistent activity is drastically slowed by excitatory coupling in a network of Hodgkin–Huxley (HH) neurons. In fact, even if the neurons are intrinsically active (say, through current injection), the excitatory coupling dramatically slows them down. We will show that the mechanism for this slowing down is a consequence of an interesting mathematical

structure (a canard) in which a trajectory passes close to a curve of points that are critical points for the intrinsic neuronal dynamics without coupling and that switch from attracting to repelling with respect to these dynamics as synaptic excitation decays [3, 22]. While delayed bifurcation resulting from slow passage infinitesimally close to such a critical curve has been studied previously [3, 15, 16, 4], we shall see that the extreme slowing that we observe involves a novel "vortex" structure and does not fit into the standard class of slow passage problems that have been considered. Indeed, the dynamics controlling the slow passage here, namely, the synaptic decay, do not need to be particularly slow for the extreme delay in activity to occur. Moreover, the slowing phenomenon occurs over a broad parameter range, which distinguishes it from typical canard scenarios.

Our results relate to those of Guckenheimer et al. [8, 9], who found prolonged interspike intervals in a model of the lateral pyloric (LP) cell of the lobster stomatogastric ganglion (see Figure 5 in [8]) and analyzed a normal form of the subcritical Hopf-homoclinic bifurcation that gives rise to this phenomenon in the LP model. To compare our work to theirs, we note that the system we study has a unique, unstable critical point, at which the synaptic variable is zero. This critical point can be made to undergo a subcritical Hopf bifurcation as certain parameters are varied, although we do not do this. It is also quite possible that we are working in a parameter regime that is near a homoclinic bifurcation curve, although we do not consider this aspect of the dynamics directly. What Guckenheimer et al. analyze, however, is not a slow passage problem. Indeed, a crucial difference arising in the present work is that the decay of the synaptic variable sweeps a critical point of a reduced subsystem through a Hopf bifurcation, whereas their analysis treats periodic orbits with the full system held at a fixed distance from bifurcation. The slow passage that we consider leads to a delayed escape from a repelling branch of critical points for the subsystem; the normal form asymptotic analysis in [9] does not involve delayed bifurcation, multiple timescales, or reduced subsystems, although a slow variable does bring trajectories closer to the Hopf bifurcation on successive oscillation cycles in the LP model. Further, we give a directly computable estimate for the change in the synaptic variable during the passage through the vortex structure that traps it, which translates directly into an estimate of passage time, and we analyze the contribution of the synaptic decay rate to the delay. The work in [9] does give an estimate for oscillation period, but this is stated in terms of normal form variables and includes some abstract constants. We note that a prolonged silent phase in the HH equations was also observed in the thorough numerical study of Doi and Kumagai [5]. There, the slowing down was attributed simply to a decrease in the instability of the unstable equilibrium of a certain fast subsystem; no further analysis was given, and the vortex phenomenon was not uncovered.

In section 2 of this paper, we begin by demonstrating the extreme delay effect, first in a large network of HH neurons, then in a reduced model, and finally in a single self-coupled neuron. Since we show that the HH networks oscillate in near synchrony, the self-coupled neuron represents a reasonable approximation of the full network behavior. In the self-coupled neuron, we show how the slowed firing rate depends on the coupling strength, the time constant of the synapses, and the reversal potential of the synapses. In section 3, we review the phase plane for the reduced HH model for a single self-coupled neuron and illustrate the slowing mechanism there. In section 4, we introduce a polynomial approximation of the model that encapsulates the behavior of the reduced HH neuron in the silent phase. We analyze this model in some detail, first showing that the usual approach to delayed bifurcations [3, 15, 16] does
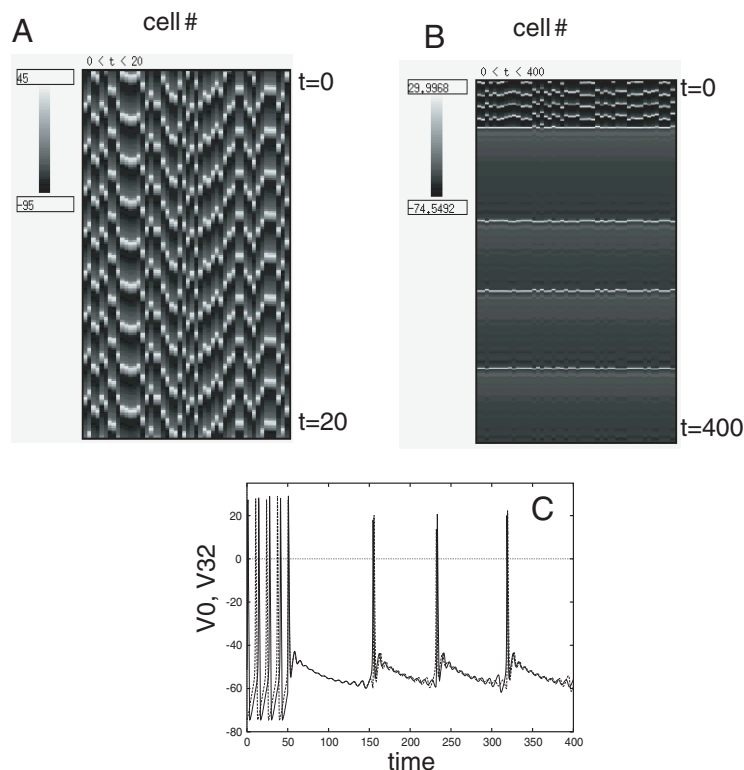
FIG. 1.1. *Behavior of networks of excitatorily coupled neurons depends on the intrinsic dynamics.* (a) *Persistent activity in a network of* 50 *cells with Traub's pyramidal cell dynamics. Neurons are indexed horizontally and time increases downward along the vertical axis. Grey scale depicts the membrane potential.* (b) *A similar network using the dynamics due to Hodgkin and Huxley. The first* 50 *milliseconds show the behavior of the uncoupled network; coupling is then turned on showing rapid synchronization and a* 10-*fold increase in the oscillation period.* (c) *Voltage traces from cells* 0 *and* 32 *(out of* 50*) from the simulation in* (b).

not capture the slowing down that we observe and then deriving a novel approach to analyze the delay, including its dependence on the synaptic decay rate. This approach focuses on the effect of a vortex structure in which the interaction of fast and slow subsystems pins trajectories in a certain neighborhood of the critical curve mentioned above. More specifically, we use this structure to derive an appropriate way-in–way-out function [3, 15, 16] that can be used to compute a good estimate of the change in the synaptic variable as a trajectory passes through the vortex. In section 5, we show how this vortex mechanism carries over to the HH system, and we explore the role of the active phase in the slow oscillations. In particular, we see how the slowing mechanism can contribute to a form of bursting, or alternation of sustained silent periods with periods of spiking, in the HH equations. Finally, in section 6, we give a further discussion of how this work relates to some earlier results and of the open questions that remain.

2. Numerical simulations of networks. If a network of excitatory cells is coupled together, often the network activity is asynchronous and has a much higher frequency than the individual cell [11, 12]. This is illustrated in Figure 1.1(a) for 50 cells coupled together in an all-to-all manner using a biophysical model for the fast

currents in a hippocampal neuron and synapses with a decay constant of 5 milliseconds [23]. Note that simulations shown in this figure, as well as all other simulations in this paper, were done using XPPAUT [7]. In the model simulated, individual cells do not fire on their own; the applied current is below threshold. However, coupled together, they produce a rhythm that is nearly 400 Hz. This is an example of strong persistent activity in an excitatory network. Contrast this behavior with another biophysical model based on the HH equations [13], with the same initial conditions and all-to-all coupling. The upper part of Figure 1.1(b) shows asynchronous output of the network when there is no coupling; the frequency is around 100 Hz. Here the neurons receive drive so that they fire spontaneously. After the first 50 milliseconds, the coupling is turned on and the network rapidly synchronizes and fires at a frequency of only about 10 Hz. Stronger coupling or longer decay rates lead to even lower frequencies. Both networks contain only three currents: a transient sodium current, a potassium current, and a leak. The individual voltage traces of two cells in Network B are shown in Figure 1.1(c). They are nearly synchronous, with out-of-phase subthreshold oscillations.

The difference in synchronization properties between these two example networks is fairly well understood, at least in the weak coupling limit. It is known that excitatory coupling can synchronize or desynchronize coupled neurons depending on many factors, such as the synaptic time constant. A very important factor is the nature of the individual neuron. In models for which the onset of repetitive firing is through a saddle node on a limit cycle (e.g., Figure 1.1(a)), excitatory coupling desynchronizes [6], while in models for which the onset is through a Hopf bifurcation (e.g., Figure 1.1(b)), excitatory coupling synchronizes [11]. As it turns out, the extreme slowing observed in the HH network also contributes to the synchronization through a form of fast threshold modulation [20]. We will return to this point in the discussion.

Our goal in much of the rest of this paper is to understand how the frequency of the synchronized oscillations is reduced to the extremely low rates observed in the HH simulations. To understand this, we first reduce the four-variable model to a two-variable system in the manner of Rinzel [18]. This will make the analysis simpler in the subsequent sections. The same network of 50 cells for the reduced system exhibits the same behavior as the full model (not shown); however, the cells synchronize perfectly, unlike in the four-variable cell model. Since synchrony (or near synchrony) appears to be a stable state of the network, we can understand the slowing down of the full network by studying a single self-coupled reduced HH cell:

$$
\begin{aligned}
C\frac{dV}{dt} &= -g_L(V - V_L) - g_K n^4(V - V_K) - g_{Na}m^3 h(V - V_{Na}) \\
&\quad + I_0 - g_{syn}s(V - V_{syn}), \\
\frac{dh}{dt} &= \frac{h_\infty(V) - h}{\tau_h(V)}, \\
m &= m_\infty(V), \\
n &= \max(.801 - 1.03h, 0), \\
\frac{ds}{dt} &= \alpha(V)(1 - s) - s/\tau_{syn}.
\end{aligned}
$$

(2.1)

The specific values of the gating functions and parameters in (2.1) are given in Appendix A. Note that the synapse has dynamics gated by the potential, V, and the reversal potential of the synapse is V_{syn}. Figure 2.1(a) shows the period of the self-coupled cell as a function of the strength of coupling, g_{syn}, for several different synaptic
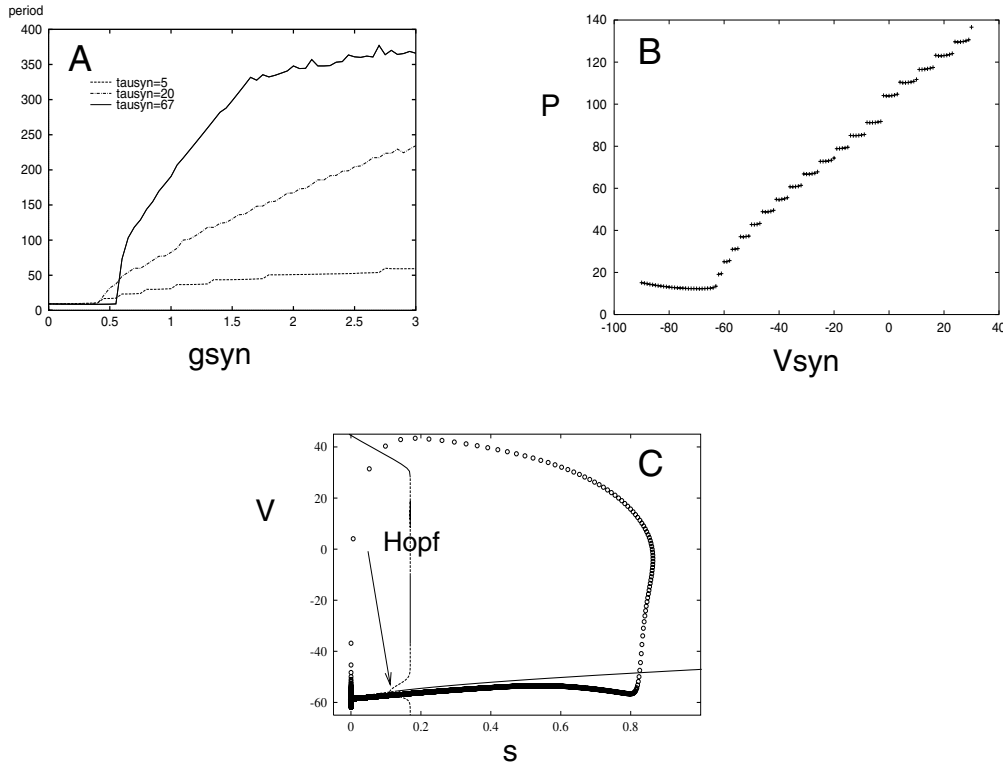
FIG. 2.1. *Properties of the self-coupled reduced HH model.* (a) *The variation of the period as a function of the maximal synaptic conductance for different synaptic decay times.* (b) *Dependence of the period on the reversal potential of the synapse;* $g_{syn} = 4\frac{ms}{cm^2}$ *and* $\tau_{syn} = 10s$*. The resting potential of the neuron is about* -65 mV*. The discontinuities in the curve occur because the trajectory cannot release until after an integral number of subthreshold oscillations (see Figure* 1.1(c)*).* (c) $V-s$ *phase plane during a slow oscillation (trajectory shown with circles and thick solid line) superimposed on the bifurcation diagram (thin solid and dashed lines) for which s is treated as a parameter. The arrow depicts the value of s at which there is a Hopf bifurcation. To compute the bifurcation diagram, we replaced the piecewise linear definition of n in* (2.1) *with a smooth approximation.*

decay rates, τ_{syn}. This dramatic slowing down is not due to simple depolarization; the period is a monotonically decreasing function of the applied current, I_0. Furthermore, for g_{syn} fixed and s held constant as a parameter, the period is roughly constant as s increases. The mechanism for slowing down depends on the transient nature of $s(t)$ and its interplay with the intrinsic dynamics of the reduced HH model. Furthermore, synaptic *excitation* is required for this; Figure 2.1(b) shows the period as a function of the reversal potential of the synapse V_{syn}.

We can give a rather crude explanation for the behavior by treating the synapse as a slow variable. Thus, in (2.1), we treat s as a parameter in the voltage dynamics. For sufficiently large values of s and for g_{syn} large, the membrane dynamics have a stable fixed point corresponding to depolarization block of the sodium current. (The resting potential is so large that the sodium channels are inactivated by the synapse.) As s is decreased, there is a Hopf bifurcation leading to large amplitude periodic solutions. Figure 2.1(c) shows the $V - s$ phase plane with the bifurcation diagram superimposed. The trajectory winds around in a clockwise motion. Essentially, the

slow oscillation is a one-spike elliptic burster [19, 24, 14]. That is, for large values of s, the resting state is stable and the neuron cannot fire. Thus, the synaptic gating variable decays. As this variable gets smaller, the trajectory passes through the Hopf bifurcation (shown by the arrow) and the resting state becomes unstable. However, as can be seen in the figure and is known to occur in elliptic bursting, the trajectory continues along the curve of unstable fixed points, to s-values well below the Hopf point, before jumping away.

While this explanation seems somewhat satisfactory, it cannot account for the drastic slowing down and extreme decay (to nearly 0) of s that we observe. Moreover, the time constant of the decay in the figure ($\tau_{syn} = 10$ msec) is not particularly slow; in this range it is about twice the decay rate of the inactivation variable, h. The mechanism for the extended period is actually quite subtle, and it turns out to be better to treat the recovery variable, h, as the slow variable and to study the dynamics in the $V - h$ plane. Moreover, we shall see that standard treatment of elliptic bursting and associated delay does not predict the extent to which the period increases with τ_{syn} here, as seen in Figure 2.1(a).

3. The $V - h$ plane. We rewrite the equations for the reduced HH model:

$$(3.1) \qquad C\frac{dV}{dt} = f(V, h) - g_{syn}s(V - V_{syn}),$$

$$(3.2) \qquad \frac{dh}{dt} = \alpha_h(V)(1 - h) - \beta_h(V)h,$$

where

$$f(V, h) = I_0 - g_{Na}h(V - V_{Na})m_\infty^3(V) - g_K(V - V_K)n^4(h) - g_L(V - V_L).$$

The equation for the synapse is

$$(3.3) \qquad \frac{ds}{dt} = \alpha(V)(1 - s) - s/\tau_{syn}.$$

While h and s have similar time courses, h evolves much more slowly than V, so we refer to (3.1) as the fast equation and (3.2) as the slow equation, and we refer to this pair of equations as (PS), for projected system. For each fixed value of s, the solution to the equation $dV/dt = 0$ forms a triple-branched curve in (V, h)-phase space, which constitutes the fast nullcline (Figure 3.1). We will also refer to the slow nullcline, given by $dh/dt = 0$ (Figure 3.1(b)). Note that as s evolves, the fast nullcline of system (3.1)–(3.2) evolves correspondingly, while the slow nullcline is independent of s. Alternatively, for the full system (3.1)–(3.3), there exist two-dimensional fast and slow nullsurfaces in (V, h, s)-phase space.

Solutions to the system (3.1)–(3.3) are strongly attracted to the left and right branches of the fast nullsurface, except during fast jumps between branches (see Figure 3.1(a)). We refer to a time period when a solution is near the left (right) branch as a silent phase (active phase). For our analysis, we will make use of projections of solutions to (V, h)-phase space, but it is important to note that s continues to evolve along with V and h.

3.1. Attraction to the intersection of nullclines and extended delay.
The left panel of Figure 3.1 shows a numerically generated trajectory of (3.1)–(3.3),
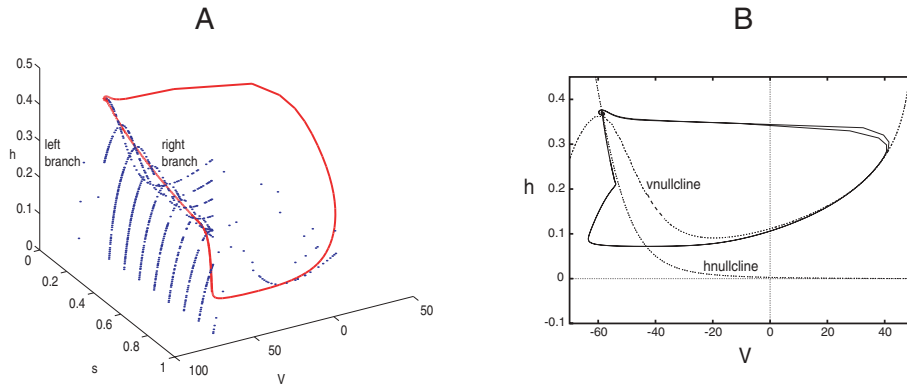
A   B

FIG. 3.1. *An orbit of* (3.1)–(3.3) *together with relevant nullclines. In the left panel, it is apparent that the orbit spends a long time in the silent phase near the left knees of the V-nullclines. In the right panel, it is clear that the orbit hugs the h-nullcline until s decays very near to zero, and then there is a small oscillation followed by a jump up to the active phase.* $\tau_{syn} = 20s$ *in this figure.*

superimposed on V-nullclines of (PS) that were numerically generated for several different values of s. A projection of this trajectory into (V, h)-phase space appears in the right panel, along with the V- and h-nullclines for an arbitrary fixed s near 0. In Figure 3.1, we see that after jumping down to the left surface of the fast nullcline, the orbit travels very close to this surface, although this is not apparent in the right panel of Figure 3.1 because we have only plotted the fast nullcline for a single, very small value of s. The orbit also appears to hug the slow nullcline as the synaptic variable s slowly decays; in other words, the orbit is very close to the intersection of the fast and slow nullclines for each fixed s. After a long delay, the orbit spirals away from the intersection of the nullclines as if this intersection point, treated as a critical point of (PS), had suddenly become unstable through a Hopf bifurcation at some small s. This is not the case; although there is a Hopf bifurcation and a loss of stability as s decays, the orbit remains near the nullcline until s reaches values well below the bifurcation point.

The intersection of the nullclines may be viewed as a critical point of (PS) with s fixed as a parameter. The stability of the critical point changes when $s \approx 0.222$ for the default parameter set, while the escape seen in Figure 3.1 occurs when $s \approx 0.003$. This means that the orbit is attracted toward the intersection (or not repelled) while that intersection represents an unstable fixed point of (PS). The objectives for this and the following section are to explain why this delayed exit occurs and to derive an analytical expression that gives a good estimate of the duration of this delay.

3.2. Ingredients for the delay. The problem presented here is that orbits appear to be attracted to a curve of unstable critical points. However, each critical point is only unstable for fixed s. For the full system (3.1)–(3.3), s decays during the silent phase, and so there are no true critical points with $s > 0$. Thus, we cannot immediately assume that the intersection will repel the orbit once it is unstable with respect to (PS). Linear stability analysis for critical points of (PS) may not be appropriate for the system (3.1)–(3.3). Somehow, one needs to take into account the dynamics of s to explain the delay in escape from the silent phase. Previous authors have contended with this issue in slow passage problems [3, 15, 16, 1, 4] and in elliptic bursting in particular [19, 24, 14, 21]. Unless $1/\tau_{syn} \ll dh/dt$, however, (3.1)–(3.3)

do not fit the standard slow passage assumptions.

Also, the h-coordinate of the fast nullcline increases as s decreases, and the slow nullcline has negative slope with respect to the variable V (in the (V, h)-plane). Thus, the intersection of the nullclines is moving up and to the left in the phase plane as s decreases. Trajectories also move in this direction, as they approach the negatively sloped slow nullcline. Thus, trajectories may approach the intersection of the nullclines, even if the linearization about the intersection of the nullclines with fixed s yields eigenvalues with positive real parts. Below, we will discuss an additional trapping mechanism that holds trajectories near this intersection.

Finally, for a value of s near the Hopf bifurcation, the nullclines are in the fold canard configuration [3]. Although this lasts for only a short period, it may provide a mechanism for a canard to arise in the full system. In this paper we will not use a singular slow-fast decomposition, and we will not use the tools of nonstandard analysis [3]. Nevertheless, the canard configuration appears to be an imperative structural feature in any system that demonstrates this extended delay, for reasons that we shall see below.

4. A simple system. To do any analysis directly, a model simpler than (3.1)–(3.3) is useful to characterize the relevant dynamics in the silent phase, although the conclusions of the analysis are expected to hold for more general systems. For the sake of analysis, the system ideally will have nullclines that are represented by polynomials. Based on the observations from the previous subsection, our model must incorporate the following characteristics:

- The slow nullcline has a negative slope with respect to the fast variable, provided the trajectory approaches the slow nullcline from the left after it enters the silent phase (see Figure 3.1). If the approach is from the right, then the slope of the curve must be positive.
- The intersection of the fast and slow nullclines is a stable critical point (when parameterized by s) of the intrinsic equations for large values of s, and then changes stability via a Hopf bifurcation induced by a transversal crossing of a conjugate pair of eigenvalues through the imaginary axis, away from the origin, as s decays. For a value of s near the Hopf bifurcation, the nullclines must be in the regular fold canard configuration, discussed in [3].
- The vector field of the system is analytic [15, 16] and autonomous during the silent phase.

4.1. The model. The model used for all analysis during the silent phase is

$$(4.1) \qquad \frac{dx}{dt} = -f(x) + y - I(s)x,$$

$$(4.2) \qquad \frac{dy}{dt} = -\epsilon \left(y + \frac{1}{4}x^5 \right),$$

$$(4.3) \qquad \frac{ds}{dt} = -\frac{s}{\tau_{syn}},$$

where $0 < \epsilon \ll 1$; note that we consider only $x < 0$. For simulations in this paper, the function f in (4.1) is

$$f(x) = \frac{1}{4}x^3 - 2x.$$

and the synaptic current function I is

$$I(s) = \frac{3}{2}s.$$

Note that this model does not oscillate, but trajectories do jump up from the silent phase. This is sufficient for consideration of behavior during the silent phase. It is not necessary to consider the active phase (when spikes occur) to explain the slow release; however, we will return to the study of the role of the active phase for the HH equations, and bursting in particular, later in the paper.

4.2. Some notation. For the remainder of the paper, the following notation will be used. $N_f(x, s)$ is the y-coordinate of the fast nullcline ($\frac{dx}{dt} = 0$) for a given x and s. Similarly, $N_s(x)$ is the y-coordinate of the slow nullcline ($\frac{dy}{dt} = 0$) for a given value of x. Note that $\partial N_f/\partial s < 0$ for $x < 0$, that $N_s(x)$ does not depend on s, and that these two curves intersect for each fixed s. Let $(\tilde{x}(s), \tilde{y}(s))$ denote the curve of intersection points.

For the system given in (4.1), (4.2), the functions $N_f(x, s)$ and $N_s(x)$ are given by

$$N_f(x, s) = f(x) + I(s)x,$$

$$N_s(x) = -\frac{1}{4}x^5.$$

The intersection of these curves is easily found for each value of s.

4.3. The usual approach. Though the trajectory is visibly separated from the intersection of the fast and slow nullclines in the right panel of Figure 3.1, it is still possible that the release value of s can be approximated using the variational equation around $(\tilde{x}(s), \tilde{y}(s))$. Indeed, this approach has been taken previously to analyze delayed escape in slow passage through a Hopf bifurcation through use of a way-in–way-out function [3, 15, 16]. This function relates the attraction of the orbit before the Hopf bifurcation to the repelling of the orbit after the change of stability has taken place. We shall see that in our case, this approach is not necessarily appropriate.

We now demonstrate the poor performance of the standard way-in–way-out, computed using the equation of first variation along the curve $(\tilde{x}(s), \tilde{y}(s))$. Let J be the Jacobian matrix of the system defined by (4.1)–(4.2) along $(\tilde{x}(s), \tilde{y}(s))$. We have that

$$(4.4) \qquad J(s) = \begin{pmatrix} -\frac{3}{4}\tilde{x}^2(s) + 2 - I(s), & 1 \\ -\epsilon\frac{5}{4}\tilde{x}^4(s), & -\epsilon \end{pmatrix}.$$

The equation of first variation is

$$(4.5) \qquad \frac{d}{ds}\begin{pmatrix} x \\ y \end{pmatrix} = -\frac{\tau_{syn}}{s}J(s)\begin{pmatrix} x \\ y \end{pmatrix}.$$

The solution to (4.5), taken from a starting point (x_0, y_0, s_{enter}), is

$$(4.6) \qquad \begin{pmatrix} x \\ y \end{pmatrix} = \exp\left(\int_{s_{enter}}^{s} -\frac{\tau_{syn}}{\omega}J(\omega)d\omega\right)\begin{pmatrix} x_0 \\ y_0 \end{pmatrix}.$$

Given an s_{enter}, we may solve the equation

$$(4.7) \qquad \left\| \exp \left(\int_{s_{enter}}^{s} -\frac{\tau_{syn}}{\omega} J(\omega) d\omega \right) \begin{pmatrix} x_0 \\ y_0 \end{pmatrix} \right\|_2 = \left\| \begin{pmatrix} x_0 \\ y_0 \end{pmatrix} \right\|_2$$

for $s = s_{exit}$. The value s_{exit} is an approximation of the value of s such that

$$\left\| \begin{pmatrix} x \\ y \end{pmatrix} \right\|_2 = \left\| \begin{pmatrix} x_0 \\ y_0 \end{pmatrix} \right\|_2,$$

where x, y are functions of s since they solve (4.5).

In typical slow passage problems [3, 15, 16, 4], this s_{exit} provides a good approximation for the release value of s. The results for the system under consideration here are not good, especially for the lower values of τ_{syn} tested. This poor performance does not contradict the standard theory; this approach breaks down precisely when the passage rate determined by the decay of s in (4.3) is not sufficiently slow in comparison with the rate of change in (4.2). The value of the approximated value of s_{exit} over a range of τ_{syn} is shown in Figure 4.1. The standard way-in–way-out analysis overestimates s_{exit}. Since s decays in the silent phase, this means that this approach underestimates the amount of time spent in the silent phase.

Notice further that the s_{exit} curve generated here is rather flat. This is expected because the linearization of the system when s is used as a parameter does not depend on τ_{syn}. The slight curvature of the s_{exit} curve that is visible in Figure 4.1 is due to the fact that different values of s_{enter} satisfy the entrance criterion (see caption) for different τ_{syn}. Simulations (solid line in Figure 4.1) suggest that the true value of s_{exit} varies as the logarithm of τ_{syn}. Correspondingly, the passage time from s_{enter} to s_{exit} grows linearly with τ_{syn}, and spike frequency decreases as $1/\tau_{syn}$ as τ_{syn} increases.

It is now apparent this is not a standard way-in–way-out problem about the curve of critical points of a slow-fast system. In the following sections, we will propose a mechanism for the increased delay, perform the corresponding analysis, and demonstrate that this approach gives a much better estimate of the observed delay than that given by the usual analysis done in this section, up to values of τ_{syn} for which $1/\tau_{syn} \ll \epsilon$. For values of τ_{syn} greater than this, the usual approach is sufficient, and as $\tau_{syn} \to \infty$ the two approaches are identical.

4.4. The trapping mechanism. As $s \to 0$, the fast nullcline moves upward in the y-coordinate, since $x < 0$ and thus $\partial N_f / \partial s < 0$. In simulations, it appears as if orbits of (4.1)–(4.3) (or of (3.1)–(3.3)) track very close to the intersection curve of the fast and slow nullclines. To understand what organizes the flow near this curve, it is useful to define the following set:

$$(4.8) \qquad A(s) = \left\{ (x_0, y_0) \left| \frac{dy}{dt}(x_0, y_0) < \frac{dN_f}{ds}(x_0, s) \frac{ds}{dt} \right. \right\}.$$

This set consists simply of the points in the (x, y)-plane such that a trajectory that passes through the point $(x_0, y_0) \in A$ travels more slowly in the vertical direction (y-direction) than does the point on the fast nullcline with the same x-coordinate. Because $N_f(x, s)$ increases as s decreases for fixed $x < 0$, we have that $\frac{dN_f}{ds}(x_0, s) \frac{ds}{dt} > 0$, which guarantees that $A(s)$ is nonempty for each s. As $x \to -\infty$, $\frac{dy}{dt} \to \infty$ as well (see (4.2)), so for each fixed y, there exists x sufficiently negative such that $\frac{dy}{dt} > \frac{dN_f}{ds} \frac{ds}{dt}$; similarly, for each fixed $x < 0$, there exists y sufficiently negative such
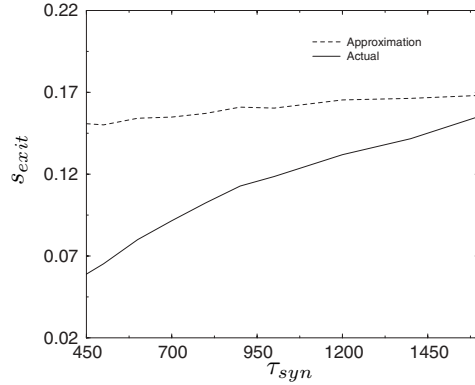
FIG. 4.1. *Values of s_{exit} computed numerically versus those computed from the usual way-in–way-out function, as τ_{syn} varies. The approximation obtained by solving (4.7) (dotted line) appears to be fairly invariant with respect to τ_{syn}, but simulations of (4.1)–(4.3) strongly suggest that this is not the case (solid line). Here, $\epsilon = .01$ and the entrance criterion used in (4.7) is $||x||_2 = 0.1$.*
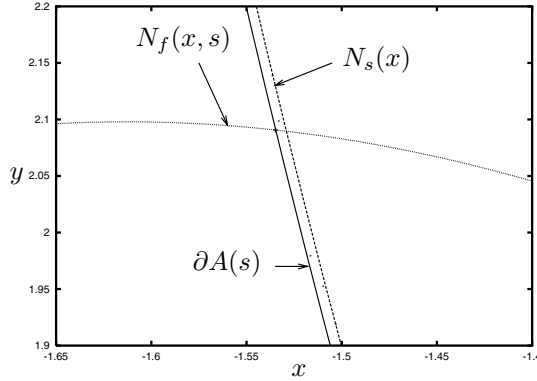

FIG. 4.2. *The curves N_f and N_s along with the boundary of the set $A(s)$ for $s = .0326$. The set $A(s)$ also includes a region to the right of $N_s(x)$, but only the shaded region is relevant.*

that this inequality holds. Thus, $A(s)$ is bounded to the left and below, and the boundary $\partial A(s)$ is a curve, which we denote $y_{\partial A(s)}(x)$, in the (x, y) plane. For the simple system (4.1)–(4.2), we can express the boundary curve $\partial A(s)$ as the graph of a function:

$$(4.9) \qquad y_{\partial A(s)}(x) = -\frac{1}{4}x^5 + \frac{3xs}{2\epsilon\tau_{syn}}.$$

Notice that $y_{\partial A(0)}(x) = N_s(x)$, and that as $\tau_{syn} \to \infty$, $y_{\partial A(s)}(x) \to N_s(x)$.

Figure 4.2 shows the curve $\partial A(s)$ for $s = .0326$, along with $N_f(x, s)$ and $N_s(x)$. For the value of s in Figure 4.2, if the trajectory lies to the right of the curve $\partial A(s)$, then $N_f(x, s)$ will be moving upward faster than the trajectory. Likewise, if the trajectory lies to the left of the curve, then the nullcline will be moving upward slower than the trajectory.

The intersection of the curves $\partial A(s)$ and $N_f(x, s)$ turns out to be extremely important for the delay phenomenon under study. The curve defined by these intersection points for a range of s values forms an attractor for values of s for which, from the perspective of the analysis done in section 4.3, the intersection of N_f and N_s
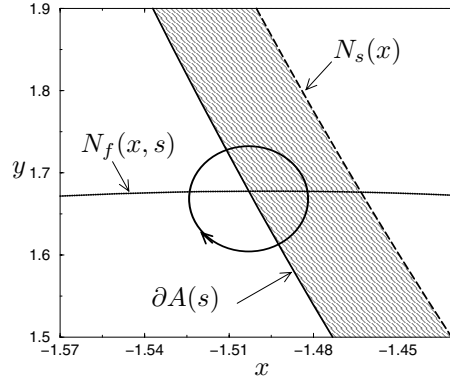
FIG. 4.3. *A sample trajectory as viewed by an observer riding the intersection of $\partial A(s)$ and $N_f(x, s)$. Trajectories to the left of $\partial A(s)$ pass to y-values above the observer, trajectories to the right fall behind. The left and right movement is dependent on whether the trajectory is above or below the curve $N_f(x, s)$.*

corresponds to a repelling set. Suppose that a trajectory lies below $N_f(x, s)$ and to the right of $\partial A(s)$. Thus, the trajectory and $N_f(x, s)$ are separating, but $\frac{dx}{dt} < 0$, and so eventually the trajectory crosses $\partial A(s)$ and then begins to catch up to $N_f(x, s)$. This may result in a net contraction toward $\partial A(s) \cap N_f(x, s)$. The y-coordinate of the trajectory will eventually increase through $N_f(x, s)$, such that $\frac{dx}{dt} > 0$ results. This causes the trajectory to again cross the curve $\partial A(s)$, and another contraction toward $\partial A(s) \cap N_f(x, s)$ may occur as $N_f(x, s)$ catches up to the trajectory. Thus, the intersection curve of $\partial A(s)$ and $N_f(x, s)$, while not itself invariant under the flow, creates a moving vortex, or core about which the flow spirals. The flow diagram around this core, projected to the (V, h)-phase plane, is shown in Figure 4.3.

This moving vortex structure generates a trapping mechanism within the flow. Simulations show that trajectories follow the vortex curve very closely during the silent phase. Using a change of variables, we next explore the stability of the vortex curve and its impact on delayed escape from the silent phase.

4.5. Equations of the moving vortex. To focus on the moving vortex, we will shift the system so that the intersection, say, $(\hat{x}(s), \hat{y}(s))$, of $\partial A(s)$ and $N_f(x, s)$ occurs at the origin for all s. For the simplified model, note that one can obtain explicit expressions for this intersection point. A linear change of variables, $z_1 = x - \hat{x}(s)$ and $z_2 = y - \hat{y}(s)$, yields the following system:

$$(4.10) \qquad \frac{dz_1}{dt} = \frac{dx}{dt} - \frac{d\hat{x}}{ds}\frac{ds}{dt},$$

$$(4.11) \qquad \frac{dz_2}{dt} = \frac{dy}{dt} - \frac{d\hat{y}}{ds}\frac{ds}{dt},$$

which can also be written

$$(4.12) \qquad \frac{dz_1}{dt} = f_1(z_1, z_2, s),$$
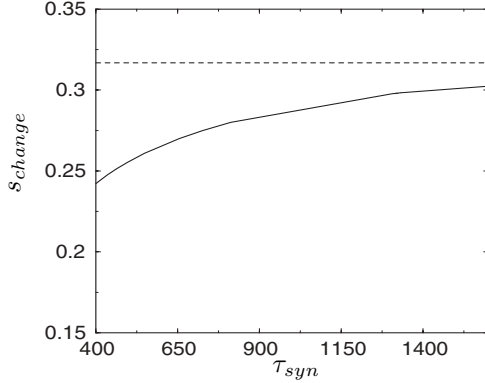
$$(4.13) \qquad \frac{dz_2}{dt} = f_2(z_1, z_2, s),$$

FIG. 4.4. *Change of stability. The solid line represents the value of s where the sign of the real part of the complex conjugate pair of eigenvalues changes along the curve $(\hat{x}(s), \hat{y}(s))$. The dotted line shows the value of s when the curve of critical points for (4.1)–(4.2) changes stability. This value is not dependent on τ_{syn}.*

where s is governed by (4.3).

If s is fixed as a parameter, then we may compute the linearization of system (4.12)–(4.13) about the vortex point $(z_1, z_2) = (0, 0)$. Although $(0, 0)$ is not a critical point for system (4.12)–(4.13), the sign of the real part of the complex conjugate pair of eigenvalues of the linearized system will still yield information about to what extent the neighborhood around the point acts as an attractor, as discussed above. Also, because the parameter τ_{syn} was incorporated into the linear component of the system during the change of variables, the value of s where the eigenvalues' real part changes sign is not invariant with respect to τ_{syn}, as it is using the regular approach discussed in section 4.3. The value of s where the eigenvalues' real part changes sign is shown in Figure 4.4. This is encouraging because it demonstrates a lower value for the change of stability in addition to a dependence on τ_{syn}, both of which are apparent in simulations but lacking in the analysis in section 4.3.

4.6. Release value for s. Because the real part of the eigenvalues crosses through zero for a smaller value of s in the linearization of system (4.12)–(4.13) about $(0, 0)$ than observed in the linearization of (4.1)–(4.2), we expect that the linearization of system (4.12)–(4.13) will provide an improved estimate of the exit value for s, relative to the analysis in section 4.3, at least until τ_{syn} becomes extremely large. In addition to the geometric argument given in section 4.4, an analytical justification for this expectation is given in Appendix B.

Now that we have transformed to the frame of the moving vortex, the analysis itself proceeds as in section 4.3. We rewrite (4.12)–(4.13) in vector form as

$$(4.14) \qquad \frac{d\vec{z}}{ds} = -\frac{\tau_{syn}}{s} \vec{f}(\vec{z}, s).$$

The equation of first variation on the vortex curve $(z_1, z_2) = (0, 0)$ is

$$(4.15) \qquad \frac{d\vec{z}}{ds} = -\frac{\tau_{syn}}{s} \vec{f}_{\vec{z}}(0, 0, s)\vec{z}.$$
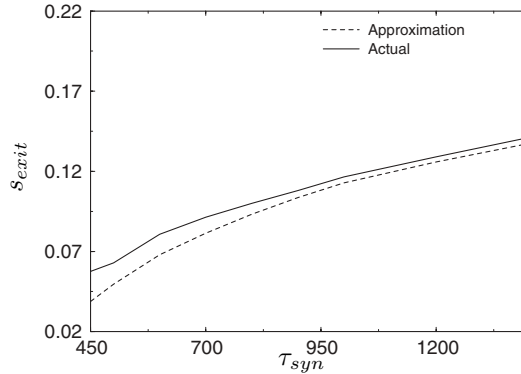
FIG. 4.5. *Improved estimate of s_{exit}. As a function of τ_{syn}, the exit value s_{exit} is derived from solution of (4.17) (dashed line) and numerical solution of the full translated model (4.12)–(4.13) (solid line). The entrance criterion for this figure was $||z||_2 = 0.03$, and again $\epsilon = 0.01$.*

The solution to (4.15) is given by

$$(4.16) \qquad \vec{z}(s) = \exp\left(-\tau_{syn}\int_{s_0}^{s}\frac{1}{w}\vec{f}_{\vec{z}}(0,0,w)dw\right)\vec{z}(s_0).$$

To approximate the value of s where release begins to occur, we choose a value s_{enter} satisfying an entrance criterion, $||z||_2 = \eta$. We solve the equation

$$(4.17) \qquad ||\vec{z}(s)||_2 = \left\|\exp\left(-\tau_{syn}\int_{s_{enter}}^{s}\frac{1}{w}\vec{f}_{\vec{z}}(0,0,w)dw\right)\vec{z}(s_{enter})\right\|_2 = \eta.$$

The results of this estimation for a range of τ_{syn} are shown, along with results from full numerical simulations, in Figure 4.5. The approximation is much better than the one obtained in section 4.3 for low to moderately high values of τ_{syn}.

Remark 4.1. In principle, there exists some curve, say, $(x_{opt}(s), y_{opt}(s))$, such that linearization about this curve yields an optimal estimate of s_{exit}. Numerical simulation suggests that system (4.12)–(4.13) has a fixed point for each s, and this is the natural candidate about which to linearize this translated system. (In terms of Appendix B, linearization about this curve would yield a truly linear system in (8.8).) However, it is not clear how to access this curve numerically, and the geometric arguments and numerical computations done here, along with the analytical calculation in Appendix B, show that the moving vortex curve is a good approximation to $(x_{opt}(s), y_{opt}(s))$ to use for estimation of s_{exit}.

Remark 4.2. Unfortunately, for very large values of τ_{syn}, the approximation loses accuracy and gives a similar, but slightly less accurate, performance to the standard approach. Recall that the moving vortex point is defined as the intersection of $\partial A(s)$ with the fast nullcline $N_f(x, s)$ for each s. The boundary $\partial A(s)$ is given by $\frac{dy}{dt} = \frac{\partial N_f}{\partial s}\frac{ds}{dt} = -\frac{\partial N_f}{\partial s}\frac{s}{\tau_{syn}}$. As τ_{syn} increases, $\partial A(s)$ therefore approaches the slow nullcline, and correspondingly the moving vortex point approaches the intersection of the fast and slow nullclines, which is exactly the moving critical point used in the standard analysis. This explains why the moving vortex analysis is similar to the standard analysis for sufficiently large τ_{syn}. However, the transformation (4.10)–(4.11) brings τ_{syn} into (4.12)–(4.13), so the two approaches remain nonidentical.
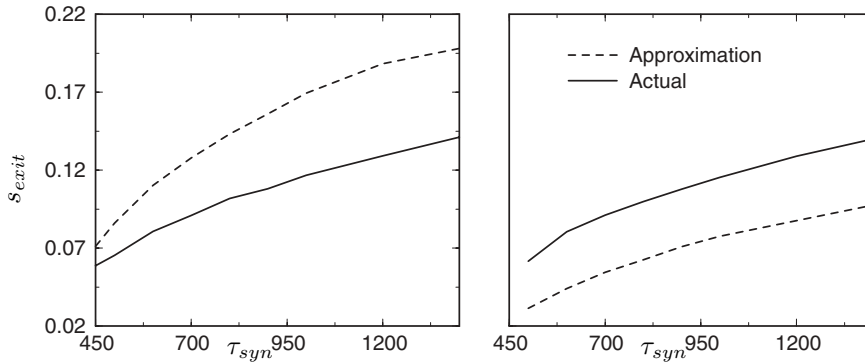
FIG. 4.6. *The approximation curve and the actual curve using the value $\eta = 0.025$ (left panel) or $\eta = 0.035$ (right panel) as the entrance criterion. The results are not as good as those in Figure 4.5.*

Remark 4.3. It is important to note that the results of our approach do depend on the value of η chosen for the entrance criterion. Because we take the equation of first variation of (4.12)–(4.13) about the vortex curve $(z_1, z_2) = (0, 0)$, rather than about the translated version of the optimal curve (x_{opt}, y_{opt}) discussed in Remark 4.1, we cannot choose η arbitrarily small. The behavior in a very small neighborhood of the origin, and the time to exit this neighborhood, do not perfectly capture the behavior near the optimal curve. Also, η cannot be chosen too large. Large η will result in failure of the approximation provided by the equation of first variation, and nonlinear terms may dominate. There must be an ideal entrance value, in the sense that the results obtained provide the most accurate approximations. Figure 4.6 shows the results derived from less appropriate values of η than that used in Figure 4.5. Note, however, that these results are still better than the standard approach (Figure 4.1) over the lower range of τ_{syn} values considered.

5. The HH equations.

5.1. Mechanism for slow oscillations. In section 4, a simplified model was used to elucidate a mechanism, involving trapping of trajectories near a vortex curve, by which slow synaptic decay results in an oscillation with a very long period. Because our simplified model satisfies the conditions listed at the start of section 4, this model is an appropriate subject for analysis, and we expect that the argument and findings from sections 4.4–4.6 carry over directly to the reduced HH model (3.1)–(3.3).

Indeed, numerical study strongly suggests that the mechanism for slow oscillations in the HH equations is identical to that of the simple model. Again, there is a vortex curve which is stable longer (for smaller s) than is the fixed-point curve created by the intersection of the fast and slow nullsurfaces. Figure 5.1 shows the analogue to Figure 4.2 for the reduced HH equations.

5.2. The active phase. Up to this point, our analysis has concerned only what occurs during the silent phase of oscillations. By changing the recovery capability of the synapse, either we can make the slow behavior discussed above more pronounced or we can eliminate the silent phase completely. The latter results in high-frequency oscillations, and for appropriate values of τ_{syn} this can induce bursting. Before discussing bursting, however, we take a closer look at how the recovery of the synapse depends on parameters in the model, assuming that a prolonged silent phase has occurred.
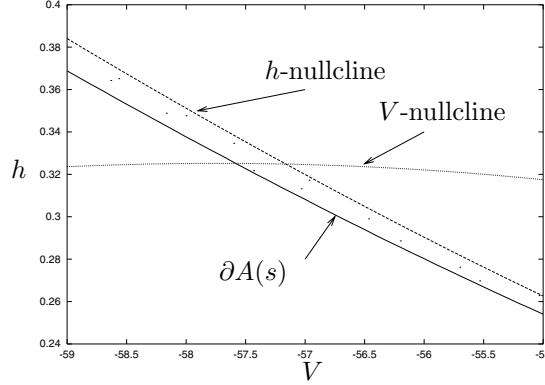
FIG. 5.1. *The set $A(s)$ for the HH equations (3.1)–(3.3) for fixed s. The shaded region is the numerically computed set of (V, h) (to the left of the slow h-nullcline) where the trajectory is moving more slowly in the direction of increasing h than is the fast V-nullcline.*

Under the flow of the reduced HH system (3.1)–(3.3), the synapse recovers (s increases) during the active phase, which begins when the cell jumps up from the vicinity of a left knee of the fast V-nullsurface and terminates when the cell jumps down from a right knee of this nullsurface. If we let $F(V, h, s)$ denote $f(V, h) - g_{syn}s(V - V_{syn})$, then the knees are the two solutions of $F(V, h, s) = \partial F(V, h, s)/\partial V = 0$, parametrized by s. More precisely, we can solve $F(V, h, s) = 0$ for $V = V(h, s)$, and then solve $\partial F(V(h, s), h, s)/\partial V = 0$ for $h = h(s)$, such that $V = V(h(s), s)$.

We can implicitly differentiate the equation

$$f(V(h(s), s), h(s)) - g_{syn}s(V(h(s), s) - V_{syn}) = 0$$

with respect to s to obtain

$$\frac{\partial f}{\partial V}\left[\frac{\partial V}{\partial h}\frac{dh}{ds} + \frac{\partial V}{\partial s}\right] + \frac{\partial f}{\partial h}\frac{dh}{ds}$$

(5.1) $$- g_{syn}s\left(\frac{\partial V}{\partial h}\frac{dh}{ds} + \frac{\partial V}{\partial s}\right) - g_{syn}(V(h(s), s) - V_{syn}) = 0.$$

Substitution of $\partial F(V(h(s), s), h(s), s)/\partial V = 0$ into (5.1) yields $\frac{\partial f}{\partial h}\frac{dh}{ds} = g_{syn}$ $\times (V(h(s), s) - V_{syn})$. Rewriting this as a formula for dh/ds and substituting the currents in f from Appendix A, as well as $V_{syn} = 0$, yields

(5.2) $$\frac{dh}{ds} = \frac{g_{syn}V}{-g_{Na}m^3(V)(V - V_{na}) - 4g_K n^3(h)(V - V_k)\frac{dn}{dh}},$$

where $V = V(h(s), s)$ and $h = h(s)$. If we insert parameter values from Appendix A, as well as the range of V values found in the silent phase (say, $h = h_L(s)$) or the active phase (say, $h = h_R(s)$), into (5.2), we find that both dh_L/ds and dh_R/ds are quite small, at most about .02. Thus, we will assume that there is a fixed value h_L of h at the jump up from the silent phase to the active phase and a fixed value h_R of h at the jump down from the active phase to the silent phase.

Now, in the active phase, we have

(5.3) $$\frac{dh}{ds} = \frac{\alpha_h(V)(1 - h) - \beta_h(V)h}{\alpha(V)(1 - s) - s/\tau_{syn}}.$$

Make the further approximations that $\alpha(V) \approx \alpha$ and $dh/dt \approx -\beta h$, for α, β constant, in the active phase, and let $\tau = \alpha + 1/\tau_{syn}$. Then direct integration of (5.3) from $(h, s) = (h_L, 0)$ to $(h, s) = (h_R, s_{max})$ yields

(5.4)
$$s_{max} = \frac{\alpha}{\tau}(1 - H^{\tau/\beta}),$$

where $H = h_R/h_L$. Equation (5.4) gives an estimate of how the level to which the synaptic variable s recovers in the active phase depends on the parameters of the HH equations, particularly α (the approximate value of $\alpha(V)$ in (3.3)), the synaptic decay rate τ_{syn}, and the active phase decay rate of h from (3.2), approximated by β.

In Figure 5.2, we compare this approximation of s_{max} to the value obtained from numerical simulation of (3.1)–(3.3) and to an alternative, naive approximation to s_{max}, namely, $\alpha/(\alpha + \tau_{syn}^{-1})$. This corresponds to the value of s that would be reached if synapses responded instantaneously to voltage. We show how s_{max} depends on α for several values of τ_{syn}, and also how s_{max} depends on τ_{syn} for $\alpha = 2$, corresponding to the default value of α_0 for the simulations in the other sections of this paper (see Appendix A). Note that there is some ambiguity in how to select the approximate decay rate β for h, since this rate typically remains near a constant value throughout much of the active phase but then decreases near the right knee, as the decay of h slows. We neglect the slowing near the right knee, which accounts for some of the error in Figure 5.2.

It is interesting to note that for fixed α, the value of s_{max} is roughly independent of τ_{syn}, such that the active phase contributes little to the slowing that occurs as τ_{syn} is increased, as discussed in the previous sections. As α increases, s_{max} increases correspondingly. This leads to a larger s_{enter} in (4.17), which in turn yields a smaller s_{exit}. Hence, the duration of the silent phase increases with α. We explore a further implication of this dependence in section 5.3.

5.3. Bursting. Consider Figure 5.3(a). This figure shows the bifurcation structure for (3.1)–(3.2) as s varies for $g_{syn} = 2$, while Figure 5.3(b) shows the voltage trace of a two-spike burst solution to (3.1)–(3.3). This solution was obtained by greatly reducing the function $\alpha(V)$, thereby reducing the turn-on of the synapse during the active (spiking) phase. Any number of spikes can be seen in a burst by scaling the recovery function appropriately.

As we have seen, during the time that a cell spends in the silent phase, its synaptic variable decays beyond the point where the fixed point (intersection of fast and slow nullclines) of the system (3.1)–(3.2) becomes unstable (s lies below the Hopf point at $s \approx 0.22$ in Figure 5.3(a)). During the active phase, the synaptic variable s increases as specified in (3.3). If s does not recover enough to reach a value for which the fixed point of (3.1)–(3.2) is stable ($s > 0.22$ in our example), then after it jumps down to the silent phase, it will not be attracted toward the slow nullcline or the vortex structure. Instead, the orbit tends toward the fast nullcline and the phase plane looks like a standard (oscillatory) relaxation oscillator. This results in a subsequent rapid jump to the active phase when the left knee of the fast nullcline is reached, corresponding to a rapid second spike, as seen, for example, at the start of the simulation in the right panel of Figure 5.3. Alternatively, if s does increase beyond the bifurcation point, then the silent phase becomes prolonged again; however, if it is still close to the bifurcation point, the silent phase duration is still reduced relative to that seen for large s, based on (4.17). Figure 5.3 shows the recovery of the synaptic variable, s, during the two-spike burst shown in the right panel of Figure 5.3.
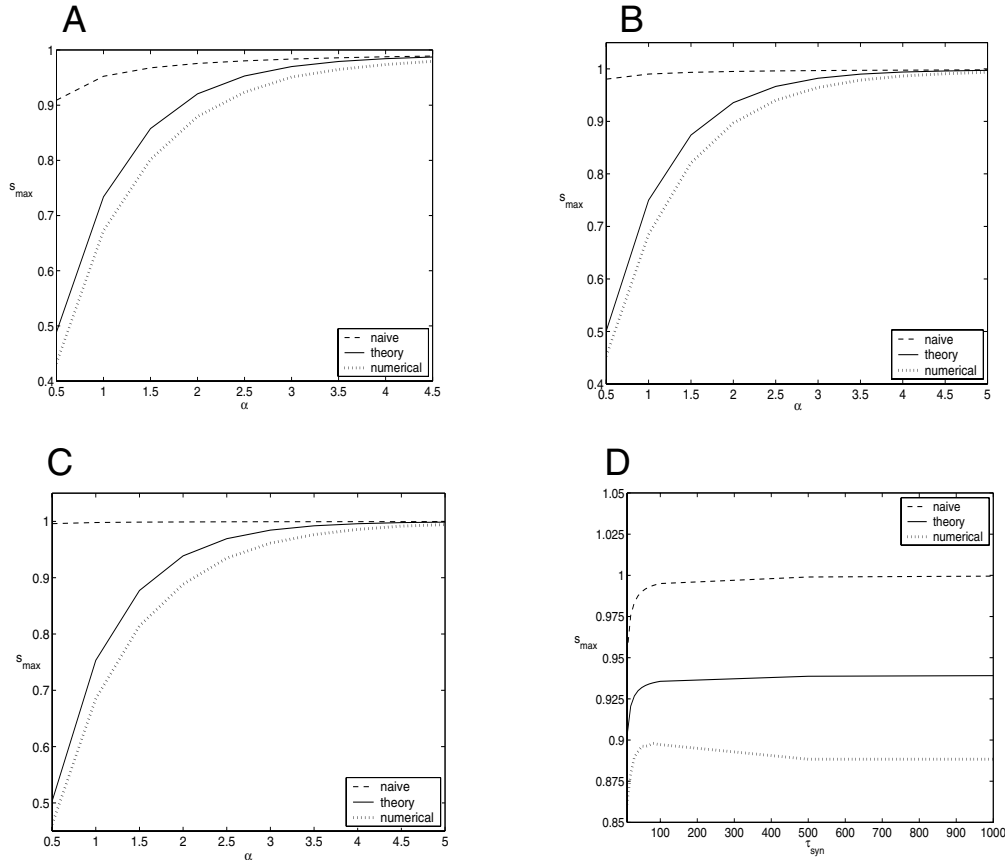
FIG. 5.2. *The dependence of synaptic recovery level, s_{max}, on the rate of synaptic rise (α) and decay (τ_{syn}). In each panel, the dashed line corresponds to the naive approximation $s_{max} \approx \alpha/(\alpha + \tau_{syn}^{-1})$, the solid line corresponds to (5.4), and the thick dotted line corresponds to the actual value of s_{max} attained in numerical simulations of (3.1)–(3.3). (a) $\tau_{syn} = 20$, (b) $\tau_{syn} = 100$, (c) $\tau_{syn} = 500$, (d) $\alpha = 2$.*

6. Discussion. It is generally assumed that synaptic connections between excitatory neurons have the effect of strengthening and accelerating neuronal firing. Indeed, part of the accepted theory of computation in cortical circuitry is that if input is strong enough to make some excitatory cells fire, then recurrent excitation among excitatory cells amplifies this activity, whereas if inhibitory input comes in before the excitatory cells can become active, then this inhibition shuts them down. In this paper, we explore a scenario in which recurrent excitation instead causes a drastic slowing of firing. We find this effect, over a broad range of parameter values, in a network of standard, biophysically derived HH model neurons, coupled with slowly decaying synaptic excitation. This highlights the important point that the effects of synaptic inputs in neuronal networks depend on the intrinsic dynamics of the cells in the network, together with the timescale of the synaptic inputs. It remains to explore the functional consequences of this result, particularly in a network of interconnected excitatory cells and inhibitory interneurons.

Since we find that synaptic excitation is strongly synchronizing in this model network (up to small differences in subthreshold oscillations), we study the mechanism behind this synaptic slowing in a self-coupled neuron. The synchronization seen here
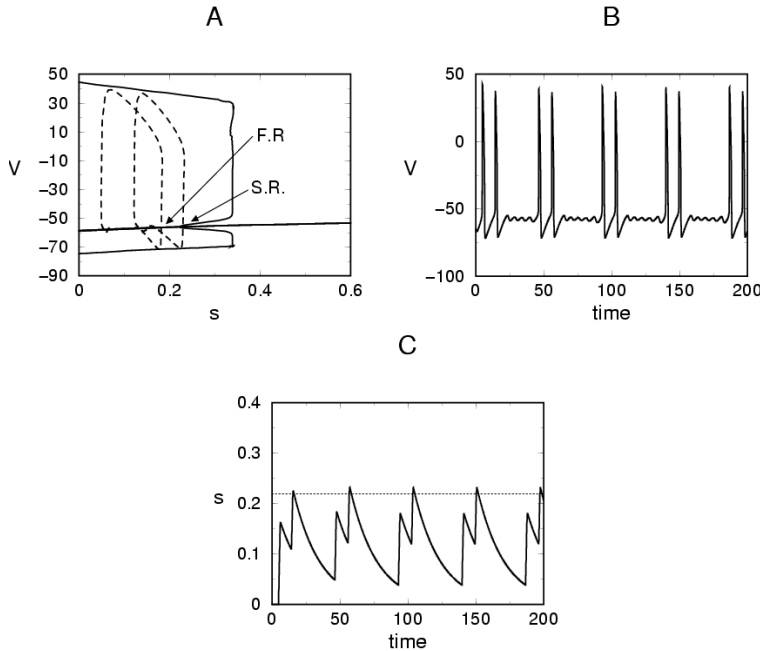
A

B

C

FIG. 5.3. *Bursting in the HH model. (a) Bifurcation diagram for the HH equations with s as the bifurcation parameter (as shown in Figure 2.1(c)). The curve at $V \approx -60$ corresponds to the critical point of system (3.1)–(3.2) formed by the intersection of the fast and slow nullclines. This becomes unstable via a subcritical Hopf bifurcation as s decreases. Here, F.R. and S.R. refer to the first and second return to the silent phase, respectively, of the dashed trajectory shown. (b) Two-spike burst solution. During the first spike of a two-spike burst, the s value does not recover enough to exit the regime where the critical point is unstable. The second recovery brings s into the stable regime, which yields a prolonged silent phase. (c) Synaptic variable, s(t) during this burst. The dashed horizontal line is the value of s where the critical point (parametrized by s) changes stability. Because this stability is necessary to obtain a cycle with an arbitrarily long period, the oscillator experiences a prolonged silent phase only once s has exceeded this threshold. Parameter values for this plot are $\tau_{syn} = 20$ and $\alpha_0 = 0.15$.*

in part results from the phase response properties of HH neurons [11]. Further, the extreme slowing in the silent phase enhances the synchronization tendency. We have seen that this slowing involves a prolonged residence near the left knee curve of a fast nullsurface. In a population of many cells in a near-synchronized state, a strong spatial compression occurs during this residence. As soon as one cell jumps up to the active phase, fast threshold modulation (FTM) [20] will pull the other cells up as well. This compression and FTM easily overwhelm any desynchronization that may occur in the other stages of an oscillation.

We use a simplified model to elucidate the moving vortex canard mechanism by which slowly decaying synaptic excitation prolongs the silent phase between spikes, and this mechanism carries over to the HH model. The scenario that we study truly meets the criteria for a canard, since the fast (V) and slow (h) nullclines of the HH model, with s taken as a parameter, are in a regular fold canard configuration for an s-value near that at which the intersection of the nullclines loses stability via a Hopf bifurcation [3]; see also [22]. Moreover, the solutions to the full system spend a significant period of time traveling along the middle branch of the V-nullsurface

(although they remain extremely close to the curve of knees; see Figure 3.1). Unlike typical canards, however, the delayed solutions that we study are easy to find, occurring over a broad range of synaptic decay rates. We do not discuss the precise size of the region in phase space from which trajectories are drawn to the vortex region, for fixed parameter values. This may relate to attraction to a stable manifold of the $s = 0$ critical point of the HH model in the vicinity of a homoclinic bifurcation, as discussed in [9], but we have not explored this issue.

According to previous analytical results, one should be able to estimate the change in the slow variable s that will occur during the silent phase by using a way-in–way-out function [3, 15, 16]. This function incorporates information from the projected system derived by treating s as a parameter. Specifically, it involves the eigenvalues of the linearization of the projected system about an appropriate curve of critical points (parametrized by s). The eigenvalues correspond to rates of decay and growth toward this critical point curve. This approach was used previously in neuronal networks to study elliptic bursting, in which there is a delayed escape from a curve of critical points that are unstable with respect to a fast subsystem [19, 24, 14, 21]. However, the novel vortex phenomenon that we have identified causes this approach to underestimate the change in s in the silent phase, and correspondingly the time spent there, for a large range of synaptic decay rates.

The vortex structure develops through a breakdown in the distinction between fast and slow dynamics in the vicinity of the critical point curve for the projected system. The corresponding flow pins trajectories near a vortex curve, which itself lies close to the curve of critical points, for a prolonged period, as the synaptic strength gradually decays. We use the vortex curve to approximate a release threshold for the synaptic variable s, relative to a specified criterion for entrance into the trapping regime. This approach makes use of a set A, determined by the dynamics of the system, that is central to the vortex effect. In particular, A relates to the relative rates of change of the nonsynaptic slow variable and the position of the fast nullcline. Note that the position of the fast nullcline depends on the size of the synaptic variable s. Further, while there are three possible timescales corresponding to the rates of change of the three dependent variables (V, h, s) in the problem, the rate of change of the nonsynaptic slow variable (characterized by ϵ) and the synaptic decay rate $1/\tau_{syn}$ are comparable over much of the range of τ_{syn} that we consider. A full mathematical analysis of the vortex mechanism, and in particular the types of vector fields and range of timescales for which computations based on the vortex curve will always give small errors, remains open for consideration.

While we introduce the vortex mechanism and perform relevant calculations in the context of a simplified model related qualitatively to the silent phase features of the HH system, we illustrate numerically that the same ingredients are also present in the reduced HH equations (e.g., Figure 5.1). Numerical simulations of the full HH model show a similar prolongation of the silent phase, with a strong dependence on the synaptic decay rate τ_{syn}; indeed, such simulations led us to note and seek an explanation for the delay mechanism in the first place. In the reduced HH equations, we connect the active phase of oscillations to the silent phase by considering how the synaptic recovery rate α affects the level to which s recovers. This affects the level of s at which trajectories enter the trapping region (quantified by our choice of η), in turn affecting our estimation of s at release from the silent phase (see (4.17)); however, as discussed in section 5.2, the level of s at release feeds back little effect on the level to which s recovers in the active phase. By exploiting our understanding of the interaction of intrinsic and synaptic dynamics, we also describe how the fast-slow

structure allows for bursting in the HH equations. While this can be considered as elliptic bursting, the burst frequency can be quite slow, as the prolonged silent phase again occurs in the intervals between bursts of spikes.

7. Appendix A. The gating functions for h in (3.2) are

$$\alpha_h(V) = .07 \exp(-(V+65)/20),$$

$$\beta_h(V) = 1/(1 + \exp(-(V+35)/10)).$$

The m and n gating variables are slaved to V and h, respectively, by

$$m = \frac{\alpha_m(V)}{\alpha_m(V) + \beta_m(V)},$$

$$n = \max(.801 - 1.03h, 0),$$

where

$$\alpha_m(V) = \frac{0.1(V+40)}{1 - \exp(-(V+40)/10)},$$

$$\beta_m(V) = 4 \exp(-(V+65)/18).$$

The synaptic recovery function, $\alpha(V)$, is given by

$$\alpha(V) = \frac{\alpha_0}{1 + \exp(-V/V_{shp})}.$$

Parameter values for all simulations are $V_{Na} = 50$, $V_K = -77$, $V_L = -54.4$, $g_{Na} = 120$, $g_K = 36$, $g_L = 0.3$, $C = 1$, $I_o = 13$, $V_{shp} = 5$, $g_{syn} = 2$, and $V_{syn} = 0$. Also, $\alpha_0 = 2$ in all sections except section 5.2, where it is varied, and section 5.3, where bursting is discussed. The units for the voltages are mV, the conductances (g_*) have units mS/cm^2, and the current (I_o) has units $\mu A/cm^2$.

8. Appendix B. Consider the model system (4.1)–(4.3), which we express as

(8.1)
$$\frac{dx}{dt} = y - N_f(x, s),$$
$$\frac{dy}{dt} = -\epsilon(y - N_s(x)),$$
$$\frac{ds}{dt} = -\frac{s}{\tau_{syn}}.$$

Note that we can express (8.1) as a pair of equations:

(8.2)
$$-\frac{s}{\tau_{syn}}\frac{dx}{ds} = y - N_f(x, s),$$
$$\frac{s}{\epsilon\tau_{syn}}\frac{dy}{ds} = y - N_s(x).$$

To find the vortex point $(\hat{x}(s), \hat{y}(s))$ about which to linearize, we solve

$$\text{(8.3)} \qquad\qquad \hat{y} = N_f(\hat{x}, s)$$

and

$$\text{(8.4)} \qquad\qquad dy(\hat{x}, \hat{y})/ds = \partial N_f(\hat{x}, s)/\partial s.$$

Together with (8.4), the second equation of (8.2) gives

$$\text{(8.5)} \qquad\qquad \epsilon \tau_{syn}(\hat{y} - N_s(\hat{x}))/s = \partial N_f(\hat{x}, s)/\partial s.$$

Implicit differentiation of (8.3) along the solution $(\hat{x}(s), \hat{y}(s))$ gives

$$\text{(8.6)} \qquad\qquad \partial N_f(\hat{x}, s)/\partial s = d\hat{y}/ds - (\partial N_f(\hat{x}, s)/\partial x)(d\hat{x}/ds).$$

Together, (8.5) and (8.6) yield

$$\text{(8.7)} \qquad\qquad \frac{d\hat{y}}{ds} = \frac{\epsilon \tau_{syn}}{s}(\hat{y} - N_s(\hat{x})) + \frac{\partial N_f(\hat{x}, s)}{\partial x}\frac{d\hat{x}}{ds}.$$

Substitute $(\hat{x}(s) + u(s), \hat{y}(s) + v(s))$ into (8.2) and linearize about $(\hat{x}, \hat{y})$ to obtain

$$\text{(8.8)} \qquad \begin{aligned} -\frac{s}{\tau}\frac{du}{ds} &= \frac{s}{\tau}\frac{d\hat{x}}{ds} + \hat{y} + v - N_f(\hat{x}, s) - u(\partial N_f(\hat{x}, s)/\partial x), \\ \frac{s}{\epsilon\tau}\frac{dv}{ds} &= -\frac{s}{\epsilon\tau}\frac{d\hat{y}}{ds} + \hat{y} + v - N_s(\hat{x}) - u(dN_s(\hat{x})/dx). \end{aligned}$$

In the first equation of (8.8), $\hat{y} = N_f(\hat{x}, s)$. From (8.7), we have

$$\frac{s}{\epsilon\tau}\frac{d\hat{y}}{ds} = \hat{y} - N_s(\hat{x}) + \frac{s}{\epsilon\tau}\frac{\partial N_f(\hat{x}, s)}{\partial x}\frac{d\hat{x}}{ds}.$$

Thus, (8.8) becomes

$$\text{(8.9)} \qquad \begin{aligned} -\frac{s}{\tau}\frac{du}{ds} &= \frac{s}{\tau}\frac{d\hat{x}}{ds} + v - u(\partial N_f(\hat{x}, s)/\partial x), \\ \frac{s}{\epsilon\tau}\frac{dv}{ds} &= v - u(dN_s(\hat{x})/dx) - \frac{s}{\epsilon\tau}(\partial N_f(\hat{x}, s)/\partial x)(d\hat{x}/ds). \end{aligned}$$

Note that while this is a linearized equation, the right-hand side is not linear in (u, v) because the vortex point is not a critical point of (8.2).

At this point, we make a key assumption. Since the trajectory lies in the vicinity of the knee during the time over which the vortex calculation is done, we henceforth assume that $\partial N_f(\hat{x}, s)/\partial x = 0$. In some sense, this amounts to assuming that the system is in a vortex canard configuration, since it specifies that the boundary $\partial A(s)$ should intersect $N_f(x, s)$ at the knee of $N_f(x, s)$. Clearly this assumption is not precisely satisfied; however, a straightforward generalization of the calculation below shows that any error resulting from the violation of this assumption will be of the same order of magnitude as $(\partial N_f(\hat{x}, s)/\partial x)(d\hat{x}/ds)$.

Next, we express $(u(s), v(s)) = (u_1(s), v_1(s)) + (\tilde{u}(s), \tilde{v}(s))$, where (u_1, v_1) is a zero of the right-hand side of (8.9) with $\partial N_f/\partial x = 0$; that is, (u_1, v_1) solves

$$\text{(8.10)} \qquad \begin{aligned} 0 &= \frac{s}{\tau}\frac{d\hat{x}}{ds} + v, \\ 0 &= v - u(dN_s(\hat{x})/dx). \end{aligned}$$

Note that $(u_1(s), v_1(s)) = O(1/\tau_{syn})$, while $(u_1'(s), v_1'(s)) = O(1/\tau_{syn})$ as well since the determinant of coefficients $(dN_s(\hat{x})/dx) \neq 0$. Substitution of this decomposition of $(u(s), v(s))$ into (8.9) yields

$$
\begin{aligned}
-\frac{s}{\tau}\frac{d\tilde{u}}{ds} &= \frac{s}{\tau}\frac{du_1}{ds} + \frac{s}{\tau}\frac{d\hat{x}}{ds} + v_1 + \tilde{v} \\
&= \frac{s}{\tau}\frac{du_1}{ds} + \tilde{v} \\
&= O(1/\tau_{syn}^2) + \tilde{v}, \\
\frac{s}{\epsilon\tau}\frac{d\tilde{v}}{ds} &= -\frac{s}{\epsilon\tau}\frac{dv_1}{ds} + v_1 - u_1(dN_s(\hat{x})/dx) + \tilde{v} - \tilde{u}(dN_s(\hat{x})/dx) \\
&= -\frac{s}{\epsilon\tau}\frac{dv_1}{ds} + \tilde{v} - \tilde{u}(dN_s(\hat{x})/dx) \\
&= O(1/\tau_{syn}) + \tilde{v} - \tilde{u}(dN_s(\hat{x})/dx),
\end{aligned}
$$

where we have assumed in the final line that $\epsilon\tau_{syn} = O(1)$. Thus, when $\epsilon\tau_{syn} = O(1)$, the error in using the equation of variations in the vortex approach is of $O(1/\tau_{syn})$.

Contrast this with the usual approach, Here one solves $0 = y - N_f(x, s)$ and $0 = y - N_s(x)$ to obtain $(\tilde{x}(s), \tilde{y}(s))$. As previously (see (8.2)), we have

$$
\begin{aligned}
-\frac{s}{\tau}\frac{dx}{ds} &= y - N_f(x, s), \\
\frac{s}{\epsilon\tau}\frac{dy}{ds} &= y - N_s(x),
\end{aligned}
$$

and we now linearize about $(\tilde{x}(s) + u(s), \tilde{y}(s) + v(s))$ to obtain, after cancellations,

$$
\begin{aligned}
-\frac{s}{\tau}\frac{du}{ds} &= \frac{s}{\tau}\frac{d\tilde{x}}{ds} + v - u(\partial N_f(\tilde{x}, s)/\partial x), \\
\frac{s}{\epsilon\tau}\frac{dv}{ds} &= -\frac{s}{\epsilon\tau}\frac{d\tilde{y}}{ds} + v - u dN_s(\tilde{x})/dx.
\end{aligned}
$$

We can apply the same decomposition of $(u(s), v(s)) = (u_1(s), v_1(s)) + (\tilde{u}(s), \tilde{v}(s))$ as above. However, if we again assume that $\epsilon\tau_{syn} = O(1)$, then we will have $(u_1, v_1) = O(1)$ from the $d\tilde{y}/ds$ term, and an $O(1)$ error can result from calculation with the equation of variations.

Acknowledgment. Thanks to F. Diener for providing material that would have otherwise been unobtainable.

REFERENCES

[1] S. M. BAER, T. ERNEUX, AND J. RINZEL, *The slow passage through a Hopf bifurcation: Delay, memory effects, and resonance*, SIAM J. Appl. Math., 49 (1989), pp. 55–71.
[2] A. COMPTE, N. BRUNEL, P. S. GOLDMAN-RAKIC, AND X. J. WANG, *Synaptic mechanisms and network dynamics underlying spatial working memory in a cortical network model*, Cerebral Cortex, 10 (2000), pp. 910–923.
[3] M. DIENER, *The canard unchained or how fast/slow dynamical systems bifurcate*, Math. Intell., 6 (1984), pp. 38–49.
[4] F. DIENER AND M. DIENER, *Maximal delay,* in Dynamic Bifurcations, É. Benoît, ed., Lecture Notes in Math. 1493, Springer, New York, 1993, pp. 71–86.
[5] S. DOI AND S. KUMAGAI, *Nonlinear dynamics of small scale biophysical neural networks*, in Biophysical Neural Networks, Mary Ann Liebert Inc., Larchmont, NY, 2001, pp. 261–297.

[6] B. ERMENTROUT, *Type* I *membranes, phase resetting curves, and synchrony*, Neural Comput., 8 (1996), pp. 979–1001.

[7] B. ERMENTROUT, *Simulating, Analyzing, and Animating Dynamical Systems: A Guide to XPPAUT for Researchers and Students*, Software Environ. Tools 14, SIAM, Philadelphia, 2002.

[8] J. GUCKENHEIMER, R. HARRIS-WARRICK, J. PECK, AND A. WILLMS, *Bifurcation, bursting, and spike frequency adaptation*, J. Comp. Neurosci., 4 (1997), pp. 257–277.

[9] J. GUCKENHEIMER AND A. WILLMS, *Asymptotic analysis of subcritical Hopf-homoclinic bifurcation*, Phys. D, 139 (2000), pp. 195–216.

[10] B. S. GUTKIN, C. R. LAING, C. L. COLBY, C. C. CHOW, AND G. B. ERMENTROUT, *Turning on and off with excitation: The role of spike-timing asynchrony and synchrony in sustained neural activity*, J. Comput. Neurosci., 11 (2001), pp. 121–134.

[11] D. HANSEL, G. MATO, AND C. MEUNIER, *Synchrony in excitatory neural networks*, Neural Comput., 7 (1995), pp. 307–337.

[12] D. HANSEL AND G. MATO, *Existence and stability of persistent states in large neuronal networks*, Phys. Rev. Lett., 86 (2001), pp. 4175–4178.

[13] A. L. HODGKIN AND A. F. HUXLEY, *A quantitative description of the membrane current and its application to conduction and excitation in nerves*, J. Physiol. (Lond.), 117 (1952), pp. 500–544.

[14] F. C. HOPPENSTEADT AND E. M. IZHIKEVICH, *Weakly Connected Neural Networks*, Springer, New York, 1997.

[15] A. I. NEISHTADT, *Prolongation of the loss of stability in the case of dynamic bifurcations.* I, Differential Equations, 23 (1987), pp. 1385–1390.

[16] A. I. NEISHTADT, *Prolongation of the loss of stability in the case of dynamic bifurcations.* II, Differential Equations, 24 (1988), pp. 171–176.

[17] D. J. PINTO AND G. B. ERMENTROUT, *Spatially structured activity in synaptically coupled neuronal networks:* I. *Traveling fronts and pulses*, SIAM J. Appl Math., 62 (2001), pp. 206–225.

[18] J. RINZEL, *Excitation dynamics: Insights from simplified membrane models*, Fed. Proc., 44 (1985), pp. 2944–2946.

[19] J. RINZEL, *A formal classification of bursting mechanisms in excitable systems*, in Proceedings of the International Congress of Mathematicians, A. M. Gleason, ed., AMS, Providence, RI, 1987, pp. 1578–1593.

[20] D. SOMERS AND N. KOPELL, *Rapid synchronization through fast threshold modulation*, Biol. Cybern., 68 (1993), pp. 393–407.

[21] J. SU, J. RUBIN, AND D. TERMAN, *Effects of noise on elliptic bursters*, Nonlinearity, 17 (2004), pp. 133–157.

[22] P. SZMOLYAN AND M. WECHSELBERGER, *Canards in* $\mathbf{R}^3$, J. Differential Equations, 177 (2001), pp. 419–453.

[23] R. D. TRAUB AND R. MILES, *Neuronal Networks of the Hippocampus*, Cambridge University Press, Cambridge, UK, 1991.

[24] X.-J. WANG AND J. RINZEL, *Oscillatory and bursting properties of neurons*, in Handbook of Brain Theory and Neural Networks, M. A. Arbib, ed., MIT Press, Cambridge, MA, 1995, pp. 689–691.